We are IntechOpen,
the world's leading publisher of
Open Access books
Built by scientists, for scientists

6,900
Open access books available

186,000
International authors and editors

200M
Downloads

154
Countries delivered to

Our authors are among the

TOP 1%
most cited scientists

12.2%
Contributors from top 500 universities

CLARIVATE ANALYTICS
BOOK CITATION INDEX
INDEXED

WEB OF SCIENCE™

Selection of our books indexed in the Book Citation Index
in Web of Science™ Core Collection (BKCI)

Interested in publishing with us?
Contact book.department@intechopen.com

Numbers displayed above are based on latest data collected.
For more information visit www.intechopen.com

Remote Sensing Application in the Maritime Search and Rescue

Jing Peng and Chaojian Shi
Shanghai Maritime University
P.R. China

1. Introduction

Maritime search and rescue (MSR- In the maritime publications, the abbreviation for search and rescue is also SAR. Here we use MSR to distinguish it from the abbreviation for Synthetic Aperture Radar.) became an enormous task with the vast growth of marine transportation and other marine activities. In the year of 2006, the MSR centers and maritime authorities in China organized and coordinated 1620 MSR operations, which involved 5322 vessels and 17498 human lives. The past few years have witnessed tremendous changes in the organizations of maritime rescue. A large part of this evolution stems from the involvement on an international scope and the contribution of the advanced technology. However, current maritime search operation, especially searching people over board, depends mostly on human eyes.

SOLAS (International convention for safety of life at sea) convention prescribes that ships must be equipped with GMDSS (Global maritime distress and safety system) equipments, which have improved the search and rescue. However, for many non SOLAS convention ships, such as fishing boats and small crafts, the detection results are not very much satisfied. With the complex sea environment, the searching of distress vessel becomes a nail-biting task. Because of the physiological characteristics of human eyes, it is difficult for the rescuer to find small target in the adverse background lighting, night or dark condition, wave or clustered seas. Continuous long time observation also causes fatigue of human eyes, resulting poor sensitivity of detection. All those factors decay the results of searching operation.

In order to improve the effect of MSR operations during the dark hours or in adverse lighting or sea conditions, remote sensing technique is a potential approach to overcome the limitation of human eyes in MSR, and thereby may hopefully improve the searching performance in complex environment or in a fatigued state of human being. Regarding ship monitoring, compared with shore-base, shipboard or airborne detecting devices, and other visible visible or infrared monitoring methods, the Synthetic Aperture Radar (SAR) remote sensing system possesses the capability of all-time, all weather, extensive and high resolution for detecting ships on the sea. Especially due to its working characteristics of not being limited by the sea surface, weather or human factors, it can detect the sea areas with geographical remote positions and hostile environment which cannot be entered directly.

In this chapter, some remote sensing techniques and algorithms concerned with the MSR are introduced. A Remote Sensing Monitoring System for Maritime Search and Rescue (RS-MSR)

is presented. This work is a part of our project—Vision Enhancement System for Maritime Search and Rescue. The main task for the RS-MSR is to acquire general information in a wider scale. The distress ship is detected and located for guiding the search operation. Surrounding ships are also distinguished to coordinate the MSR operation. Some important data such as current and sea state are retrieved to help decision-making of the operation. Section 2 proposes the outline of the remote sensing methods for maritime search and rescue; Guided by the systematic functions and structures of the RS-MSR described in Section 2, Section 3 introduces the related algorithms used in RS-MSR. Section 4 describes the architecture of the remote sensing aided system for maritime search and rescue. The experiment design and the implementation performance are given in Section 5. Finally, Section 6 concludes the paper.

2. Outline

The primary role of the remote sensing is to provide a secondary source of information for the MSR operations. A remote sensing monitoring system can, to some extent, overcome the shortcomings and inadequacies of human eyes. It can also improve the searching speed and accuracy, and is of significance in promoting rescue success rate and efficiency. It can aid the rescuers to fulfill the task of search and rescue, especially for small targets, such as persons in distress and life boats, and could provide a good detection and identification result.

2.1 Introduction to the system functions

According to the requirement of search and rescue, a Remote Sensing Monitoring System for Maritime Search and Rescue (RS-MSR) is designed. Table 1 illustrates the main functions of a RS-MSR system.

RS-MSR System demand	Function
Satellite transit inquiry	Satellite transit inquiry
Ship detection	1) Ship position detection 2) Ship type identification/classification 3) Ship size estimation 4) Ship heading/direction estimation
Sea state analysis	Wave direction and estimation

Integrated processing	1. Non-remote sensing data fusion
	  - VTS (Vessel Traffic Services) report
	  - AIS (Automatic Identification System) report
	2. Performance analysis
	  - Recognition rate
	  - Identification/classification rate
	  - Position error
	3. Rescue position prediction
	  - Time prediction
	  - Ship speed and velocity
	  - Predict the rescue area according to the heading/ direction of the distress ship and the sea state

Table 1. The main functions of a RS-MSR system required

2.2 Algorithm introduction

According to the requirement of the maritime search and rescue, the Synthetic Aperture Radar (SAR) imageries are used for this purpose. The algorithms concerned with the system demand are introduced as follows.

2.2.1 Distributed target detection method in the Gaussian scale-space

In the SAR images with high resolution, each target occupies several resolution units to form area target. So detecting the ship target in the SAR images with high resolution should regard the target as distributive target, and the assumption of point target under the traditional radar is not suitable any more. The project here proposes a distributed target detection method in the Gaussian scale-space. The distance relationship among the detected objects is adopted to identify the distributed target. In the situation of hardly estimating the background's scattering distribution or of low SNR (signal-to-noise ratio), this method can realize the distributive target detection more effectively than CFAR method.

2.2.2 Ship size category estimation model

In the SAR images with high resolution, the ship target can be divided into three categories according to their dimension, among which small ships(≤50m) are represented as point target, while the middle size ship(≤100m) as distributive target of single corner and big size ship(≥100m) as double corner distributive target. According to the relative positions of the corner and combining the orbit information (resolution ratio and incident angle) of the SAR image, the length, height and the direction of the ship will be worked out.

2.2.3 Ship location correction and ship direction estimation method

The imaging geometry of the SAR imagery is slant-range projection. So, due to the geometric distortions, such as layover, foreshortening, and shadows, there exits measurement error between the observed position and its actual location. In this method, using the directional texture of the wake of ship, the convergent point of the wake pattern can be calculated, which is the actual location of the stern. Then the position correcting parameters can be worked out.

A bow wave is the wave that forms at the bow of a ship when it moves through the water. As the bow wave spreads out, it defines the outer limits of a ship's wake. Theoretically, the convergent point of the bow wave' outline must at the extended line of the ship's heading. The vanishing point can be calculated by the Hough transform, and the heading direction of the ship can be calculated according to the coordinates of the bow and the stern.

2.2.4 Wave direction estimation based on the partial energy direction

Wave direction estimation can be used to analyze the sea state of the target area and supply basis for search and rescue area decision. This method is set up on the basis of steerable filter, which is a filter set composed of an even-symmetric filter and an odd-symmetric filter. When the orthogonal filter set is rotated to the same orientation of the local texture, the oriented energy reaches its maximum. The orientation corresponding to the maximum

oriented energy is defined as the dominant orientation of the local energy at that point. And the main direction of the wave can be estimated.

2.2.5 The registration algorithm of SAR image and nautical chart based on Gaussian principle curve

To ensure precise detection and location of the distressed ship in the MSR, the navigational chart and the remote sensing image should be matched beforehand. Because the SAR image and the electronic chart are data from different sensors, the content and intensities of these images are much different from each other. Coastline is a stable and reliable feature for navigation in coast area. However, the deformation between edges extracted from different signals may produce position errors, and the noise in radar signals may greatly influence the edge extraction result. And how to obtain reliable control-points and how to obtain the correct correspondence are the key issues in the registration algorithm. In this chapter, a multi-scaled registration algorithm for SAR image and electronic chart is presented. Based on the scale-space theory, coastlines from the two images are matched in both frequency domain and image domain with continuous scale level.

3. Algorithms and methods in the maritime search and rescue

3.1 Distributed target detection method in the Gaussian scale-space

In the high resolution SAR images, the large-scale ship and super large-scale ship (>100 meters) are presented as distributed targets. In this algorithm, these targets are detected by the distance relationship between the echo intensity of the masthead light and the ship hull. The detection of distributed target based on location-dependent information can be completed by two-step detection. In the first step, the ship target is characterized in the Gaussian scale-space. This transforms the signal range value into binary. Then, the detection of the singular objects is implemented using constant false alarm rate(CFAR), and record the location of the pixel point whose value is 1. The second step aims at finding the distributed target from the result of the first step detection by applying location-dependent information.

3.1.1 Ship characteristic description

Under the ideal condition, in the $z(x)$ of the image which has its background gray value as 0, there is a maxima value h and strong scattered point $f_b(x)$ with width as w. Considering the edge effect of the image, we build the mathematical model as follows:

$$f_b(x) = \begin{cases} h(1-(x/w)^2), & |x| \le w \\ 0, & |x| > w \end{cases} \tag{1}$$

The responses of these spot-like targets in Gaussian scale space are presented as $r_b(x,\sigma,w,h)$:

$$\begin{aligned} r_b(x,\sigma,w,h) &= g_\sigma(x) * f_b(x) \\ &= \frac{h}{w^2}[(w^2 - x^2 - \sigma^2)(\phi_\sigma(x+w) - \phi_\sigma(x-w)) \\ &\quad -2\sigma^2 x(g_\sigma(x+w) - g_\sigma(x-w)) - \sigma^4(g'_\sigma(x+w) - g'_\sigma(x-w))] \end{aligned} \tag{2}$$

Among them, $\phi_\sigma(x) = \int\limits_{-\infty}^{x} e^{-\frac{x^2}{2\sigma^2}} dt$.

In order to departure the ship target from the grey scale space, we define a Gaussian comparison function $e_b(x)$. If the responses of $f(x)$ in Gaussian scale-space is $r(x,\sigma, w, h)$, then we have:

$$e_b(x) = \begin{cases} 1, & r(x,\sigma,w,h) \leq f(x), \text{ and } |x| \leq w \\ 0, & \text{other} \end{cases} \tag{3}$$

Then, the detection of the singular target is implemented by way of constant false alarm rate(CFAR).

3.1.2 Distributed target detection based on location-dependent

Set the SAR image as a $N_R \times N_A$ matrix, where N_R and N_A represent the dimension of range and azimuth respectively, and use $\{i_{R1}, i_{R2}, \cdots, i_{RK}\}$ as range coordinate and $\{i_{A1}, i_{A2}, \cdots, i_{AK}\}$ as azimuth coordinate separately for convenience.

The detected relative distance among different scattered units can be defined.

$$d(j,k) = \|i_j - j_k\|, k > j, j = 1, 2, \cdots, K - 1 \tag{4}$$

where $\| \|$ means norm. Equation(4) represents the relative distance between two scattered units j and k, and it expresses the location relations among each target pixel point after the Gaussian scale-space detection.

When the range and the azimuth are considered separately, the distance can be defined as

$$d(j,k) = \left(\left| i_{Rk} - i_{Rj} \right|, \left| i_{Ak} - i_{Aj} \right| \right) \tag{5}$$

Due to the geometric distortions of the SAR image, the ship hull and the mast will occupy several resolution units in the image. Set a candidate ship target M_0 (M_0 includes the ship hull and the mast), where M_{0R} and M_{0A} represent the size of M_0 in the range direction and the azimuth direction respectively. Set a bounding box with size of $M_{0R} \times M_{0A}$, which is the smallest rectangle containing the detecting ship. Assume that the size of the detecting target is $S_R \times S_A$ and the radar resolution is $\Delta R \times \Delta A$, then $M_{0R} \times M_{0A} = \frac{S_R}{\Delta R} \times \frac{S_A}{\Delta A}$.

Regarding to the distributed targets, at least M scattering points will be detected after the second detection step, and then M can be defined as the distance threshold d_{th} within the distributed target.

$$d_{th} = M = \mu M_{0R} \times M_{0A} \tag{6}$$

Here $\mu \in (0,1)$ is the confident coefficient and it is determined by the empirical data of the radar echo.

Define the size of the distributed target T_s as:

$$T_s = d(M_0, (0,0)) \tag{7}$$

Equation (7) defines the distance from the position of the bounding box M_0 to the origin point (0,0). The distance describes the size of the detecting target, which is related to the form of the distance definition.

According to the size of the bounding box M_0 and Equation (6), the number of scattered points (marked as u) of each target reference window and their locations (i.e. target location) can be calculated as follow.

$$\left.\begin{array}{ll} u \geq d_{th}, & \text{target} \\ u < d_{th}, & \text{non} - \text{target} \end{array}\right\} \tag{8}$$

Under the definition in Equation (7), $d(T_{position}, i_k)$ and T_s are all two-dimension data, we need define its output. Set $T_s = (T_{sR}, T_{sA})$, $d = (T_{position}, i_k) = (d_R, d_A)$, and then the export definition of $d(T_{position}, i_k) > T_s$ is:

$$d = (T_{position}, i_k) > T_s = \begin{cases} 1, & \text{other} \\ 0, & d_R \leq T_{sR} \text{ and } d_A \leq T_{sA} \end{cases} \tag{9}$$

3.1.3 Algorithm realization

According to the above description of the algorithm, to design the integrated detection algorithm based on two-dimension location-dependent information, the procedure is shown as follows:

1. Initially set $k = 1$, $u = 1$, and the position of the target centre is $T_{position} = i_k$;

2. If $d = (T_{position}, i_k) \leq T_s$, the number of pixels contained in the current target is $u = u + 1$, and renew the central position of the current target $T_{position} = \dfrac{(u-1)T_{position} + i_k}{u}$;

3. If $d = (T_{position}, i_k) > T_s$, then create a new target with its central pixel location as $T_{position} = i_k$, $u = 1$;

4. Traversal searches the image.

3.2 Ship size category estimation model

In the SAR images with high resolution, the ship target can be divided into two categories according to their dimension. The small ships are represented as single corner target while big ships as double corner distributed targets. According to the relative plane location of the double corner and combining the orbit information (resolution ratio and incident angle) of SAR images, the parameters of the ship's status, such as the length, height and the heading direction can be calculated. Table 2 shows the corresponding incident angle of ENVISAT ASAR.

Image Position	Breadth (km)	Distance to the Substellar Point (km)	Incident Angle (°)
IS1	104.8	187.2 − 292.0	15.0 − 22.9
IS2	104.8	242.0 − 346.9	19.2 − 26.7
IS3	81.5	337.2 − 418.7	26.0 − 31.4
IS4	88.1	412.0 − 500.1	31.0 − 36.3
IS5	64.2	490.4 − 554.6	35.8 − 39.4
IS6	70.1	549.7 − 619.8	39.1 − 42.8
IS7	56.5	614.7 − 671.1	42.5 − 45.2

Table 2. Corresponding incident angle range of ENVISAT ASAR

Build a space coordinates as Fig.1 with the true north (Y axis) as the reference direction. The ship length is l, and the width is w, height is h, azimuthal angle of the bow is α (the angle between the bow and the North), and then a ship model can be descripted by a set of geometric parameters as $P = [\alpha, l, w, h]$. For example, if the satellite is descending, for ENVISAT ASAR it is a right view image. Set radar incident angle as θ, the azimuthal angle as β (the angle between the satellite and the true north) and the height as H, which is shown as in Fig.1. According to SAR imaging mechanism, the shadow in the figure shows the ship's scattering image, which is determined by the ship's ground position, shape and the radar's scattering orientation. Assume that the ship hull scattering length is s and the width is d. The range is

$$w = b\cos(\beta - \alpha)$$

$$b = d\tan^2\theta \tag{10}$$

$$w = d\tan^2\theta\cos(\beta - \alpha)$$

Here w is the ship width, b is the width of the ship at the radar range, d is the scattering width of hull target，θ is the radar incident angle, β is the radar azimuthal angle and α is the bow azimuthal angle. The azimuth is

$$s = l\cos(\beta - \alpha)$$

$$l = \frac{s}{\cos(\beta - \alpha)} \tag{11}$$

$$w = d\tan^2\theta\cos(\beta - \alpha)$$

Here l is the ship length and s is the scattering length of the ship target images at the radar range, β is the radar azimuthal angle and α is the bow azimuthal angle.

According to the length of the ship ships can be divided into small-sized (<50 meters), mid-sized (50-100 meters), big-sized (100-200 meters) and extra big-sized ship (>200 meters).
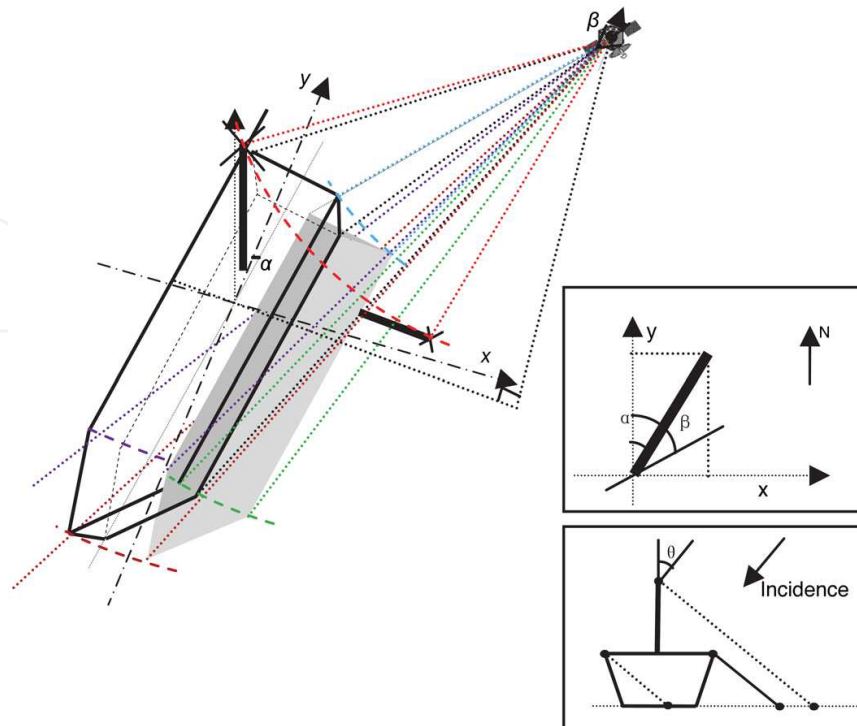
Fig. 1. The ship geometric projection model in the SAR image

3.3 Ship positioning correction and direction estimation

3.3.1 Ship positioning correction

Due to the geometric distortions of the SAR imaging, there exits measurement error between the observed position and its actual location. With this method here we can get the real position of the stern by way of detecting the ship's wake region with directional texture and calculating the convergent point of the ship's wake. Thereby, the position correcting parameter will be worked out. This method enables us to get the information of wave-making of the distressed ship when the wake profile is invisible or in violent sea status, which improves the flexibility and automaticity for understanding the marine remote sensor images.

3.3.1.1 Wake region determination

A wake is the directional texture formed on the water surface immediately behind the ship. Therefore, the mean direction of the wake is consistent with the ship heading. In this algorithm, regarding the ship as the center, we divide the sea surface of the ship's neighborhood into several partially overlapped sectors. Define the angle between the edge of the sector and the positive direction of X axis as the edge direction angle of the sector, and the two edge direction angles formed by two edges of sectors are defined the direction range of the sector areas, and the median of the two edge angles is the main direction of the sector area. Calculate the textural energy of the main direction in each sector area of the ship, and set the sector area with the most textural energy as the wake areas. The direction range of the sector is regarded as the wake direction range, and the target area close to the wake range is the stern in the image.

3.3.1.2 Course calculation

In the wake area, calculate the textural direction pixel by pixel, and set the pixels whose textural directions belong to the wake direction interval as the wake points. Use the least-square method to calculate the mean direction of the wake, and the result is defined as the direction of the ship's wake, i.e. the course.

3.3.1.3 Actual lactation of the stern

Theoretically, a wake is the region of disturbed flow immediately behind the ship, and the texture of the wake pattern should converge to a point which is the real position of the stern. Collect the wake points in the wake region. Use the Hough transform to calculate the vanishing point of the wake texture. And this point is regarded as the actual location of the stern.

3.3.1.4 Projection offset calculation

According to the actual position of the stern and its image position, the projecting offset can be calculated. Use the stern offset, the projecting model is built. After calibration, the original detected result can be modified and the actual location of the ship target can be obtained.

3.3.2 Heading direction estimation method

A bow wave is the wave that forms at the bow of a ship when it moves through the water. As the bow wave spreads out, it defines the outer limits of a ship's wake. Theoretically, the convergent point of the bow wave' outline must be on the extending line of the ship's heading. The convergent point can be obtained by the Hough transform, and the heading direction of the ship can be calculated by the positions of the bow and the stern. Using the orbit information (resolution ratio and incident angle) of SAR images, the length, height and the direction of the ship can be worked out. The heading direction vector is defined in accordance with the bow wave's outline, which points from the actual location of the stern to the convergent point of the bow wave. Then, the heading direction is defined as the direction between the heading direction vector and the true north in anti-clockwise.

3.4 The registration algorithm of SAR image and nautical chart based on Gaussian principle curve

To implement registration to remote sensing images with navigational radar image and the chart, the detection results will be directly showed both on the remote sensing image and the chart, and then do contrast verification among the remote sensing detection results and the data of radar and AIS. A multi-scale matching algorithm of radar image and chart is proposed in this project, transforming the coastline into a set of smooth curves in the Gaussian scale space, and making coarse to fine image registration to radar image and the coastline in the chart separately in the frequency field and the spatial field.

3.4.1 Curve feature representation

In the extracting coastlines, many near-shore objects such as ships and navigation marks that also have strong echoes may be merged by mistakes, leading to Ω-shaped spurs of the

coastlines. In order to reduce the influence caused by this kind of noises, a geometric criterion is proposed to avoid selecting initial seeds on spurs. To find proper seed, each candidate seed on the rough coastline is considered by means of judging the angle between the candidate seed and its adjacent selected seed from a certain point on the land, which is the mirror of the radar image center, i.e., the own-ship position. This procedure is illustrated in Fig.2. Search for the follow-up seed to seed v_i in the counter clockwise direction along the initial coastline, where O is the own-ship position, and O' is its mirror point perpendicular to the course. Judge the angle $\tilde{\theta}_i$ between v_i and the candidate point $\tilde{v}_{i+1}$ from O'. Spur may occur when $\tilde{\theta}_i$ is small or even negative. Bypass those kinds of points $\tilde{v}_{i+1}$ until meet a point v_{i+1} whose angle θ_i with v_i is larger than a predefined threshold.
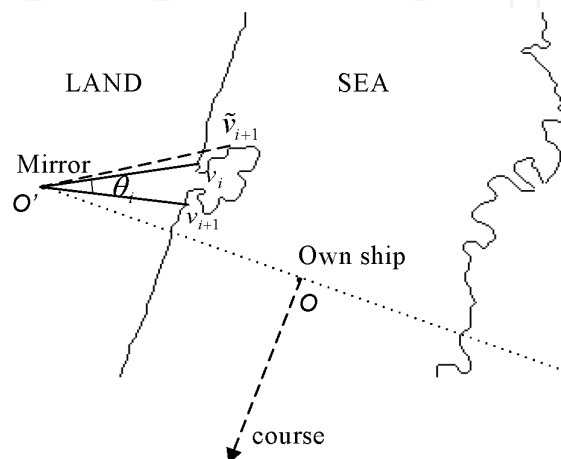
Fig. 2. Dispose the burr noise of radar coastline

Then, a family of smoothed coastlines is derived in the Gaussian scale-space, as shown in Fig.3. Scale-space is a special type of multi-scale representation that comprises a continuous scale parameter and preserves the same spatial sampling at all scales.

$$L(.;\sigma) = g(.;\sigma) * f \tag{12}$$

where the Gaussian kernel is $g_\sigma(x) = [\exp(-x^2/2\sigma^2)]/\sqrt{2\pi}\sigma$. Because the coastline in the electronic chart is rather smooth, the scale-space derivation is only done for the SAR image.
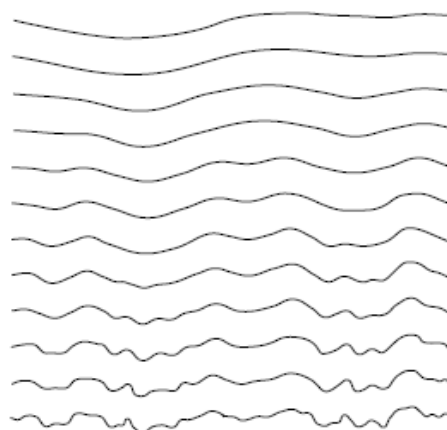
Fig. 3. Continuous smooth coastline in different scale spaces

3.4.2 Registration

3.4.2.1 Coarse registration in the phase domain

The image registration technique based on Fourier-Mellin transform finds its applications in many different fields thanks to its high accuracy, robustness and low computational cost. It can be used to register images which are misaligned due to rotation, scaling and translation. The basic theory for translation estimation is the Fourier shift theorem. Denote

$$\mathcal{F}\{f(x,y)\} \overset{\Delta}{=} F(w_x, w_y) \tag{13}$$

which is the Fourier transform of $f(x,y)$. Then

$$\mathcal{F}\{f(x+\Delta x, y+\Delta y)\} \overset{\Delta}{=} F(w_x, w_y)e^{j(w_x\Delta x + w_y\Delta y_0)} \tag{14}$$

And the image translation can be estimated by the cross-spectrum of the two images.

$$\frac{F_1(u,v)F_2^*(u,v)}{\left|F_1(u,v)F_2^*(u,v)\right|} = e^{j(w_x\Delta x + w_y\Delta y_0)} \tag{15}$$

Assuming $s(x,y)$ is transformed image of $r(x,y)$ after translation $(\Delta x, \Delta y)$, rotation α and scaling σ (in both x and y directions).

$$s(x,y) = r[\sigma(x\cos\alpha + y\sin\alpha) - \Delta x, \sigma(-x\sin\alpha + y\cos\alpha) - \Delta y] \tag{16}$$

And $s(x,y)$ will gain a two-dimensional pulse at the position of $(\Delta x, \Delta y)$ in the (x,y) space. Then, the relation between the corresponding Fourier transform of $s(x,y)$ and $r(x,y)$ is:

$$s(u,v) = e^{-j\phi_s(u,v)}R[\sigma^{-1}(u\cos\alpha + v\sin\alpha), \sigma^{-1}(-u\sin\alpha + v\cos\alpha)] \tag{17}$$

And the corresponding amplitude spectrum is:

$$|s(u,v)| = \sigma^{-2}\left|R[\sigma^{-1}(u\cos\alpha + v\sin\alpha), \sigma^{-1}(-u\sin\alpha + v\cos\alpha)]\right| \tag{18}$$

Then, the rotation angle and the scaling factor can be calculated in the log-polar coordinates.

$$s_{p1}(\theta, \log\rho) = r_{p1}(\theta - \alpha, \log\rho - \log\sigma) \tag{19}$$

And evidently, s_{p1} will gain a 2-D pulse at (α, σ) in the Hemi-Polar-Log $(\theta, \log\rho)$ coordinates. The phase-correlation method computes the transformation parameters by taking the curve as a whole, which takes the advantage of low computation cost and a good ability of noise immunity. This procedure is repeated in the Gaussian scale-space with a set of decreasing observing scales, and the two images are registered from rough to precise. And the transformation parameters are evaluated by clustering based on the evidence theory.

3.4.2.2 The selection of control point and registration seed

The derived curve is transformed into graph, and the weight of each node is represented by the energy defined by,

$$E_\sigma = w_i \sigma^2(v_i, v_{i-1}) = w_i \left[\sum_{x \in v_i v_{i-1}} (C_\sigma(x) - \bar{C}_\sigma(x))^2 \right] \tag{20}$$

where C_σ is the Gaussian curvature under scale σ defined by the coined product of the largest and the smallest curvatures of $\overline{v_i v_{i-1}}$.

$$C_\sigma(v_i, v_{i-1}) = L_{vv} L_w = L_{xx} L_y - 2L_x L_y L_{xy} + L_{yy} L_x \tag{21}$$

where L_i is the Laplacian operator. C_σ turns out to be a good corner detector, which is an important invariant feature to describe the structure of a derived curve in certain scale-space. And scaled energy E_σ is a three-order vector, which describes the variance of curvature.

The nodes with big E_σ are selected as control points. On the local straight line points the Gaussian curvature is zero, and the connections of these points form a parabolic line. Then, every two adjacent parabolic lines construct a registration curve fragment. This method assures each seed curve contain the typical topology of the local region.

3.4.3 Precise registration based on the principle curve graph

The Hausdoff distance is adopted as the comparability metric, and the best matching feature curve fragment is obtained by using the minimum distance classifier. This procedure is repeated in the Gaussian scale-space with a set of decreasing observing scales, and the two images are registered from coarse to fine. The Haussdoff distance between the registration curve N_1 and the reference curve M_1 is defined by Equation(22).

$$D_{Haussdoff}(N_1, M_1) = \max(d_F(N_1, M_1), d_B(N_1, M_1)) = \max_{L_j \in N_1} \min_{L_i \in M_1} \left(\left| L_i - L_j \right| \right) \tag{22}$$

If $D_{Haussdoff}(N_1, M_2) \le \varepsilon$, then the two curves are matched. ε is a given threshold. The matching metric is shown as Fig.4.
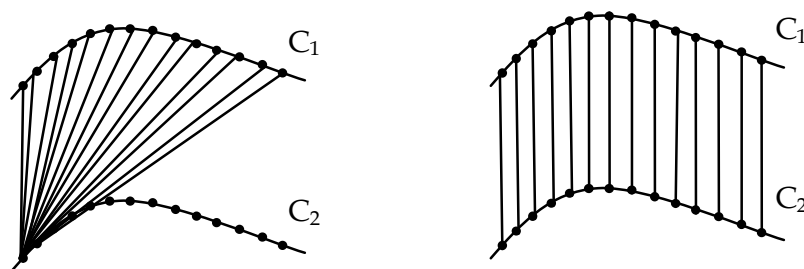

Fig. 4. The Haussdoff distance metric

3.4.4 Experiment analysis

The experimental images are obtained at a narrow channel in Yangzi River, China, May 1st, 2007. The own ship's position (OS POSN) is [32°13.525 N, 119°40.368 E], at speed of 13.8 knots and on course of 235.0°. The electronic chart of this area is a version in 2002. Many new docks are built, and moreover, the inland electronic chart in China uses the Gauss-Kruger coordinates, while the radar image uses the projected polar coordinates. Different coordinate systems also add extra deformation between the two images.

We choose a series of image sections from the electronic chart as the reference image, and take the radar image as image to be matched. The chart sections are selected along the coastline with a half size of the chart. And the registration is done between the chart section and the radar image. Because the two images are from different sensors, the coarse registration in single scale cannot carry out a prominent pulse in the $(\theta, \log \rho)$ space, as shown in Fig. 5. The registration procedure is repeated at scale levels $\sigma = 2^i, i = 1, \cdots, 6$. Then, the estimated transformation parameters are clustered as $(\hat{\theta}, \hat{s}, \hat{t}_x, \hat{t}_y) = [-1.9, \ 0.344, \ 353, \ 725]$.
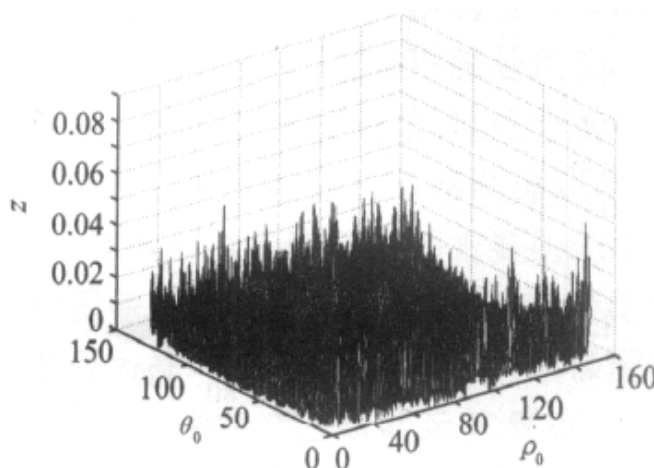
Fig. 5. The IFFT of spectrum in single scale

Twenty-one pairs of control points are selected from both the derived SAR image and the chart at the scale level of $\sigma = 16$. Using the Housdoff distance metric, the transformation parameters of second registration are obtained as $(\hat{\theta}, \hat{s}, \hat{t}_x, \hat{t}_y) = [-1.9, \ 0.357, \ 371, \ 660]$.

The registration results are shown in Fig.6. The registration performance is evaluated by manually registering a remote sensing image from the Google Earth with the nautical chart. The registered image is at [32°13.369 N, 119°40.279 E], 7m distance from its true position, and the rotation bias is -1.1°. The result proves that our method is feasible. Errors come from the strong echo of various objects near the shore.

3.5 Wave direction estimation based on local energy orientation

This method is based on Gabor filter. According to Morrone and Owens theories, local energy is the image mean square response of filter set formed by an even symmetry filter M_e and an odd symmetry filter M_o, and it gets the biggest local energy value at singular points, such as edges and corners.
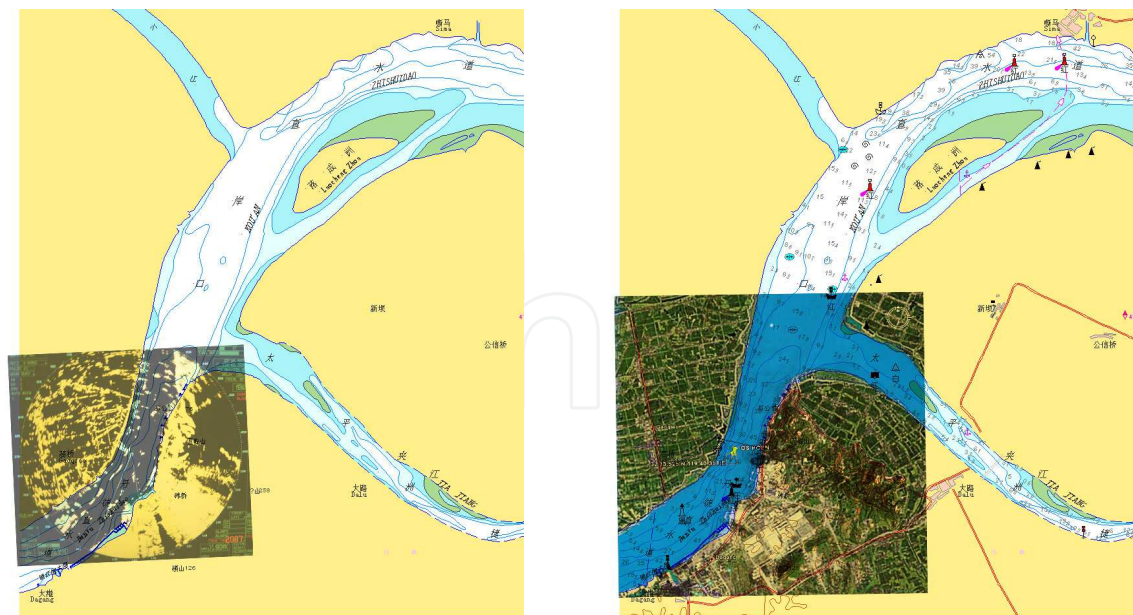
Fig. 6. Registered image pairs. (left) radar image and nautical chart, (right) remote sensing image and nautical chart

$$E(x,y) = \sqrt{(M_e * f(x,y))^2 + (M_o * f(x,y))^2} \qquad (23)$$

The steerable filter is the linear combination of a set of base filters, which are partially overlapped in the frequency domain, and can be rotated. An orthogonal filter pair is a combination of a steerable filter and its Hilbert transformation, which is designed to detect precisely the features of the edge, texture and singular point of the target. To obtain the 2-D local energy in continuous frequency space, the Wavelet Transform is used to decompose the signal into a series of sub-band signals with particular frequencies. Here we use the Mexico-hat wavelet G_2 to build the steerable filter G_2^θ:

$$G_2^\theta = k_1(\theta)G_2^0 + k_2(\theta)G_2^{\pi/3} + k_3(\theta)G_2^{2\pi/3} \qquad (24)$$
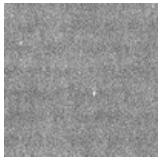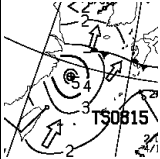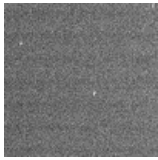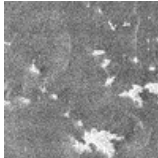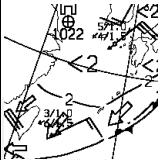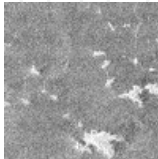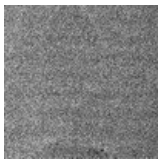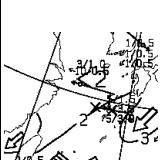
The Mexican-hat wavelet $G_2(x,y) = \partial^2 \exp[-(x^2 + y^2)]/\partial x^2$ is a symmetric filter with sharp narrow bandwidth, thus it can effectively restrain noise and enhance the signal in particular frequency, and it is common used in multi-scale edge detection. The fundamental filters G_2^0, $G_2^{\pi/3}$, $G_2^{2\pi/3}$ represent the forms of G_2 rotating to 0, $\pi/3$, $2\pi/3$, respectively. $k_i(\theta)$ is the interpolation function corresponding to the fundamental filters. Then, the form of G_2 in any orientation is represented by the linear combination of G_2^0, $G_2^{\pi/3}$, $G_2^{2\pi/3}$. We can get the direction energy of arbitrary pixel (x,y) of the image in an arbitrary direction θ by using the orthogonal filter bank formed by steerable filter G_2^θ and its Hilbert transformation H_2^θ.

$$E^\theta(x,y) = \sqrt{(G_2^\theta * f(x,y))^2 + (H_2^\theta * f(x,y))^2} \qquad (25)$$

As for the singular characteristics, e.g. the edge, when the orthogonal filter moves to the same direction with this characteristic, the direction energy reaches maximum value. The corresponding direction of the local orientation energy is called the principal direction of the pixel's local energy.

The wave image is filtered in this algorithm to eliminate speckles by way of Lee filter, and on this basis the principal energy direction of the wave can be estimated.

The experiment uses the satellite ENVISAT-1 ASAR data of 30th Sep. to 19th Oct, and the experimental area covers 30°48′N ~ 31°20′N, 122°10′E ~ 122°47′E. We use the wave direction estimation based on local energy direction to calculate the wave direction for AP polarization data. The calculation results are compared with the JMH wave analysis chart from Japan Meteorological Agency. Table 3 shows the experiment result of this wave
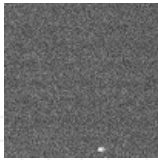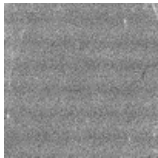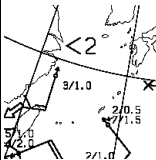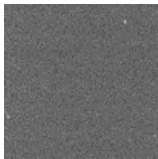
Acquisition Time (UTC)	Image	Polarization Mode	Wave Direction	Direction Energy	Incident Angle	Estimated Direction	JMH Wave Analysis
2008-09-30 13:53		VV	0°	124.3043	41.1016	75.1857	
			30	117.9377			
			60	132.5371			
			90	135.8590			
			120	131.9720			
			150	118.6072			
		VH	0	111.2229			
			30	116.8233			
			60	133.8221			
			90	136.7364			
			120	132.8555			
			150	116.2534			
20081008 01:50		HH	0	78.0928	33.9364	104.2056	
			30	97.9058			
			60	130.5053			
			90	145.1742			
			120	130.5707			
			150	99.4210			
		VV	0	77.5663			
			30	99.3430			
			60	133.5955			
			90	146.8708			
			120	133.2834			
			150	99.9747			
20081010 13:39		HH	0	14.0134	19.2636	99.9323	
			30	33.8942			
			60	133.1682			
			90	268.4664			
			120	132.8741			
			150	34.1923			

Acquisition Time (UTC)	Image	Polarization Mode	Wave Direction	Direction Energy	Incident Angle	Estimated Direction	JMH Wave Analysis
		HV	0	7.7873			
			30	19.1000			
			60	74.9717			
			90	153.2269			
			120	75.1100			
			150	18.9022			
20081019 13:56		HH	0	120.3329	44.0092	104.8161	
			30	115.1276			
			60	120.3069			
			90	116.8428			
			120	120.2216			
			150	118.1973			
		HV	0	66.6512			
			30	69.6033			
			60	73.6283			
			90	71.8446			
			120	73.2198			
			150	69.0945			

Table 3. The experiment result of the wave direction estimation algorithm

direction estimation algorithm. The experimental result analysis shows that VV polarization mode is the best way for wave analysis, and the following is HH, while cross polarization VH and HV mode are not ideal.

4. The architecture of the remote sensing aided maritime search and rescue system

The Remote Sensing Monitoring System for Maritime Search and Rescue (RS-MSR) consists of four modules including satellite transit inquiry module, vessel detection module, sea state analysis module and integrated processing module. Ship detection module has three functions and they are ship location, ship type identification/classification and ship movement direction estimation. Sea state analysis mainly estimates the wave direction. The integrated processing module receives the detection results from ship detection module and sea state analysis module. According to the distressd ownship' position, heading and the wave direction, combining the time used for data receiving, it estimates the position of the distressed ship, and combining the satellite parameter, it can revise the result obtained through ship detection. The analytic result by way of integrated processing module can be transmitted to the Maritime Safety Administration (MSA) and the rescue vessel on the working field, providing assisting decisions of areas for the rescue work. Fig. 7 describes the architecture of RS-MSR.
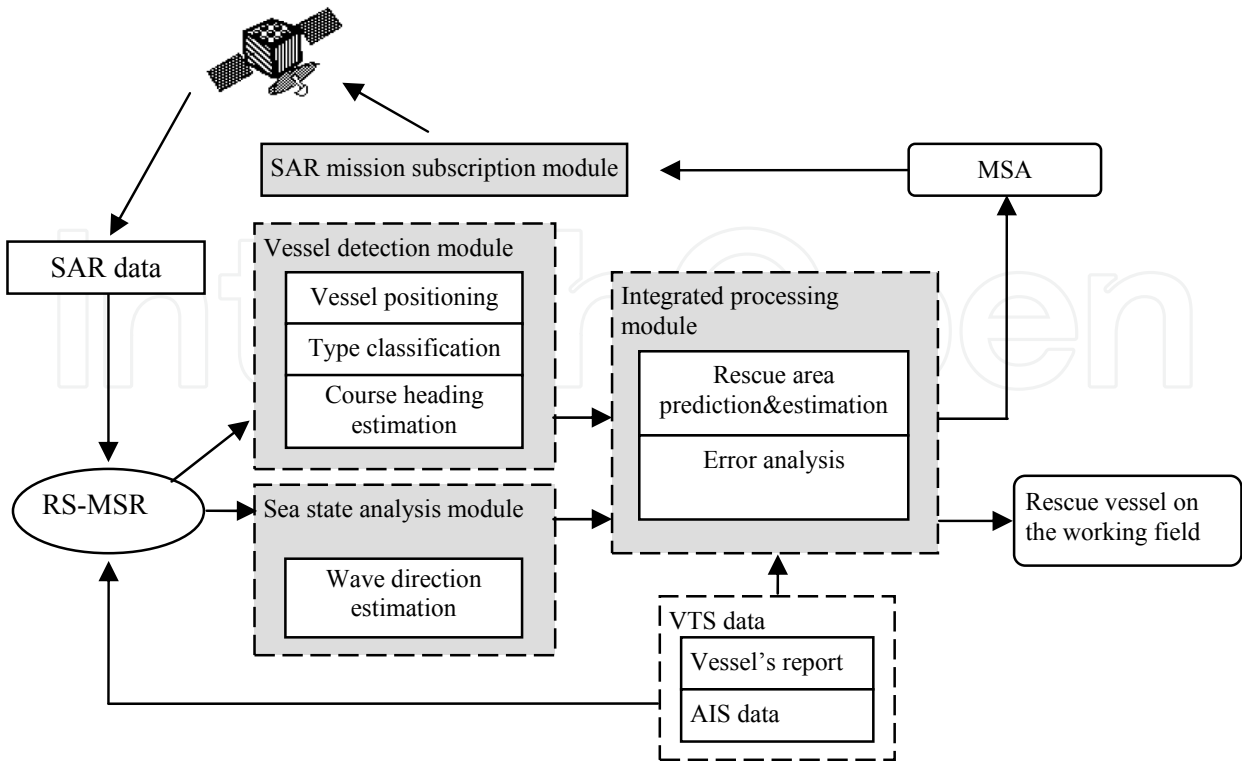
Fig. 7. The architecture of the Remote Sensing Monitoring System for Maritime Search and Rescue (RS-MSR)

4.1 Satellite transit inquiry module

With the development of astronavigation, the number of satellites installed with SAR sensors is increasing. Facing with so many satellites with different purposes, it has become a tough problem for clients to judge and select what they want quickly. RS-MSR sets up a real-time satellite coverage inquiry system including the commonly used satellites around the world, such as RadarSat, Envisat, ERS, CosmoSAR, TerraSAR, helping clients to retrieve quickly the crossing time and the orbit data of these satellites at specific area.

4.2 Ship detection module

Ship detection module is the core unit of the whole RS-MSR system. Using the micro-area images of distressed areas supplied by way of satellite, it can detect and monitor the ships and the accidental areas, supplying clue of the distressed ship for search and rescue and helping to determine the areas quickly. This module consists three parts including: (1) ship detection; (2) ship classification/identification; and (3) ship direction and course estimation.

4.3 Sea state analysis module

Sea state analysis module can perform initial analysis on the situation of the distressed area by estimating the wave direction and supply foundation for search and rescue decision, which is useful for estimating the floating direction and location of the distressed ships.

4.4 Integrated processing module

The integrated processing module is mainly used for follow up processes of the detection result and search and rescue assisting forecast. It has two main functions. Firstly, search and rescue range estimation. According to the current location, navigation direction and the wave direction, estimate the potential searching areas of the distressed ship under the settled speed of the ship and velocity of flow. Secondly, ship location correction. Combine the satellite parameter to revise the error caused by slant-range projection imaging of the SAR images. The analysis data obtained by way of integrated processing module can be saved as *.dat or *.mat form and transmitted to marine department and the rescue spot, supplying assistant for the rescue areas determination.

5. System experimental performance

5.1 Experiment design

In our experiment, the *Yangtze River* estuary (Changjiangkou) precautionary (30°48′N ~ 31°20′N, 122°10′E ~ 122°47′E) is selected as the experimental working zone (Fig. 8). This region includes the inward and outward fairway of the *Yangtze River* estuary and the 1# and 2# anchorages. The *Yangtze River* estuary is a tide-coordinated region, and the tide rise and fall twice per day. The tidal range is up to 4 meters. And the flow is rapid. Both anchored ships and underway ships are aggregated at this place. Casualties happen often, and it is a key region for the monitoring of maritime search and rescue. Therefore, this place is an excellent experimental region.
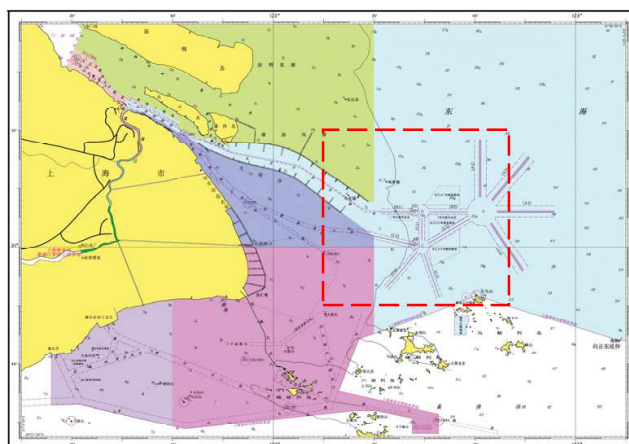

Fig. 8. The experimental working zone in the nautical chart

5.2 Experiment data

From 2008.09.30 to 2008.10.19, we took four times of experiments. EnviSat-1 ASAR data is used in this experiment. Data acquisition is implemented considering the three tidal conditions: rise, fall and still. And the data includes: VTS maritime Radar, AIS, weather information, tide and flow, etc. The details are listed in Table 4. Here we present the experiment on 2008.10.19 as an example.

- Experiment region: 30°48′N~31°20′N, 122°10′E~122°47′E
- Experiment time: from 2008.09.30 to 2008.10.19

-      Tide reference: Jigujiao *tide*-gauge station (31°10'24″ N, 122°22'54″ E)
-      Flow reference: Xinkaihe *tide*-gauge station (31°14'36″ N, 121°29'12″ E)

No.	Experiment Time (UTC)	Tide reference (Jigujiao)	Flow reference (Xinkaihe)
1	2008-09-30, 13:53:24	14:00 L, 431cm	10:00 L, 105cm/s
2	2008-10-08, 01:50:45	02:00 L, 244cm	10:00 L, 105cm/s
3	2008-10-10, 13:39:00	14:00 L, 303cm	22:00 L, -076cm/s
4	2008-10-19, 13:56:17	14:00 L, 246cm	22:00 L, 077cm/s

Table 4. The hydrological information in the experiment

5.2.1 The remote sensing data

Data: ASA_APP_1PNBEI20081019_135613_000000202073_00082_34705_4038.N1
Polarization Mode: HH/HV
The detail information is listed in Table 5.

Mode	Track	Frame	Lower Left longitude	Upper Right longitude	Upper Left latitude	Lower Right latitude	Swath	Passing direction	Start Date /Time (UTC)
APP_H H/HV	82	596	122.167	122.921	31.6478	30.7285	S7	Descending	2008-10-19 13:56:18.802

Table 5. The detail information of the remote sensing data

5.2.2 The VTS reference data

The radar data and AIS data are received from the VTS center of Shanghai port. Fig. 9 is the VTS shore-based radar detection picture simultaneously at the acquisition time of the remote sensing data. The VTS report shows the name and position of all the vessels equipped with AIS in the Yangtze River estuary. The Radar data and AIS data provide a reference for the performance analysis of the system experiment.
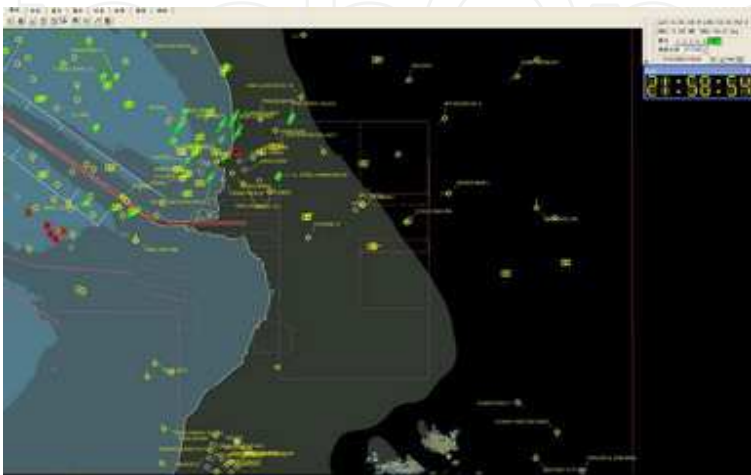

Fig. 9. The VTS report at the passing time of the satellite (2008-10-19, 13:56:17 UTC)

5.2.3 The weather information

The weather information includes the JMH weather chart, wave height, flow rate, and the tidal data. Fig. 10 shows the track of the No.15 typhoon (30 September, 2008).
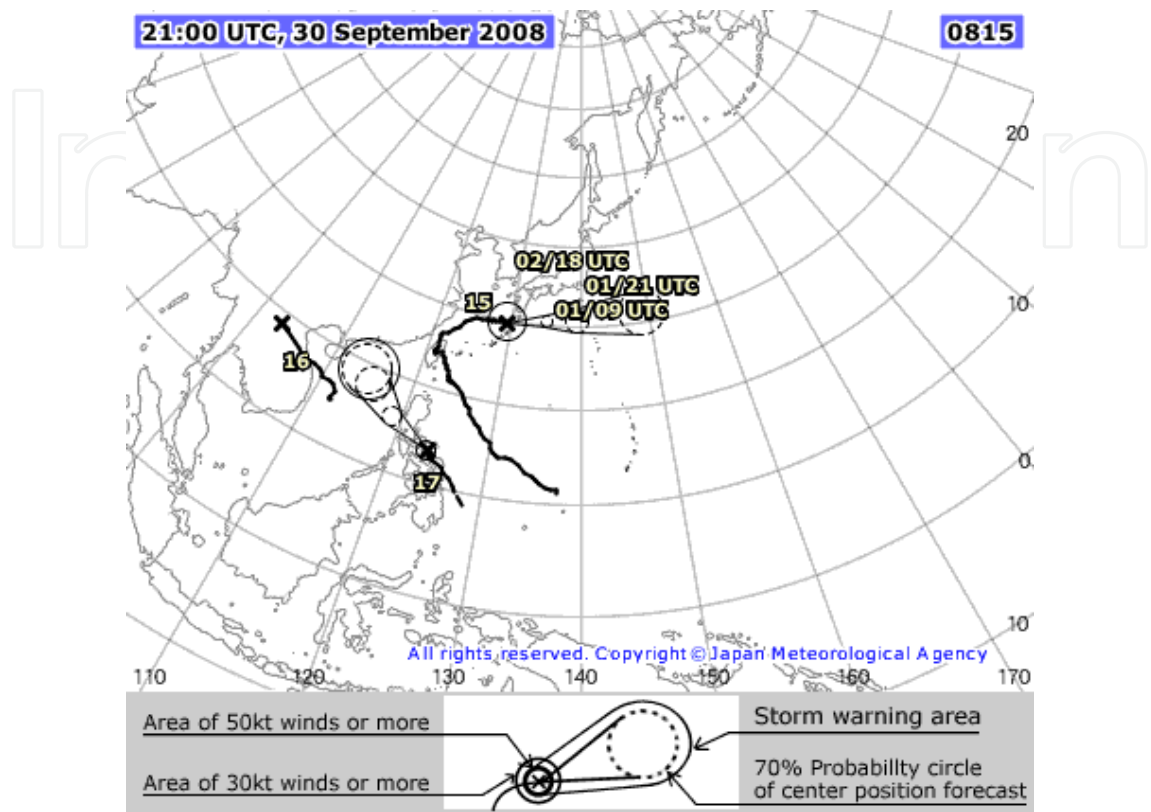

Fig. 10. The track of the No.15 typhoon (30 September,2008)

5.3 System experiment

Here we set detecting zone as follow:

- UpperLeft longitude: 122.338E
- UpperLeft latitude: 30.9261N
- Range in longitude: 9.8276 nmile
- Range in latitude: 8.96046 nmile

Fig. 11 presents the working interface of the Remote Sensing Monitoring System for Maritime Search & Rescue (RS-MSR). And Fig. 12 shows the original SAR image.

5.3.1 Vessel detection

Vessel detection includes: ship position detection, type identification, length estimation and heading estimation. The detection results are shown in Fig. 13(middle) and Table 6. The ship type classified into four categories: small, middle, large, and extra-large. The ship heading direction is the angle between the ship heading and the real north in clockwise.

In Fig. 13(right), the red circle represents small ship (point target) and the green arrow indicates the estimated heading direction of big ship (distributed corners).
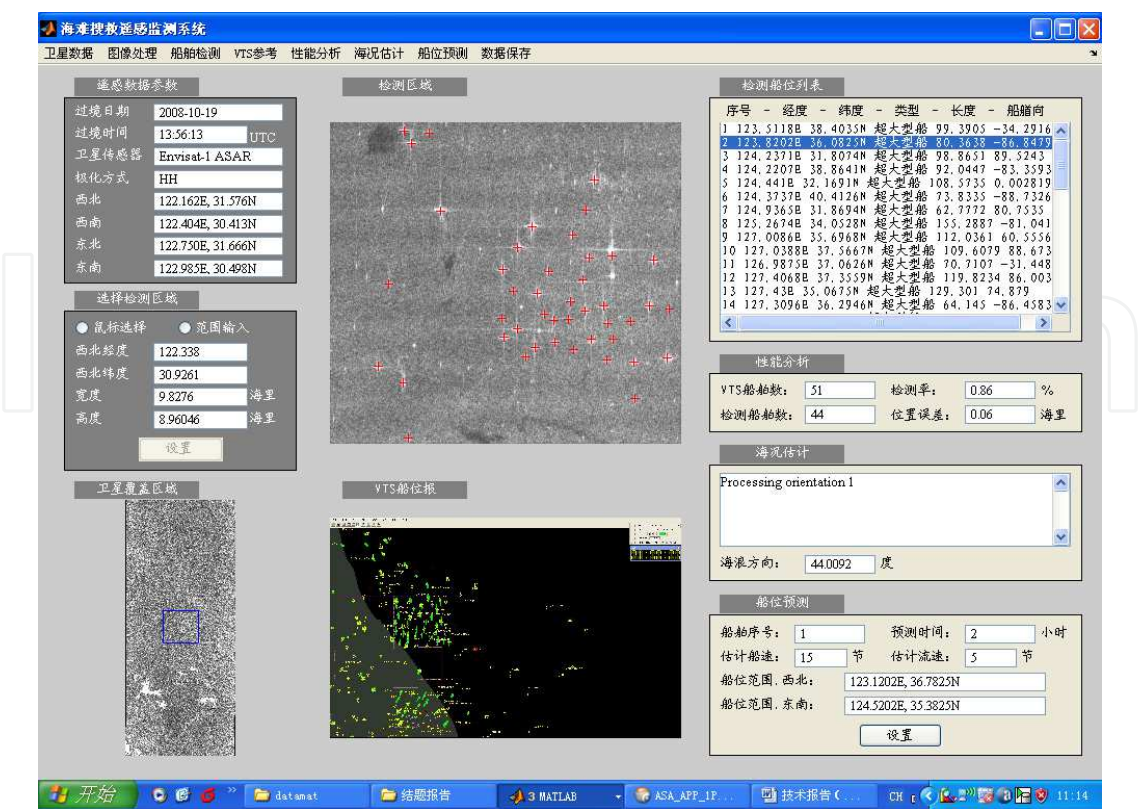
Fig. 11. The working interface of the Remote Sensing Monitoring System for Maritime Search & Rescue (RS-MSR)
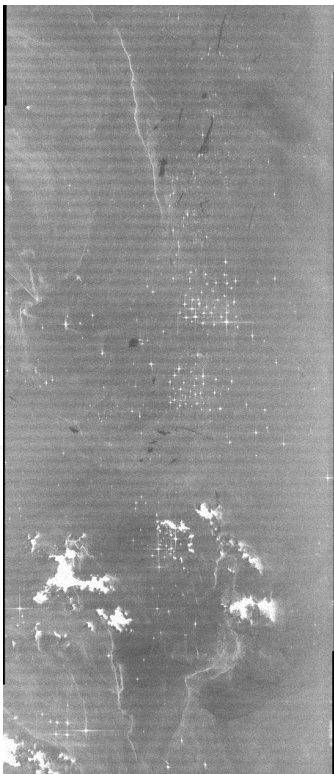

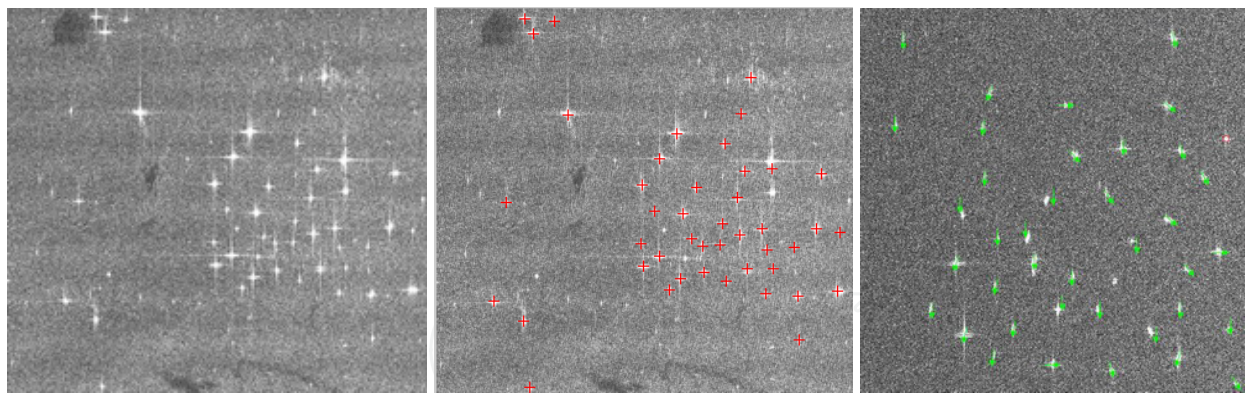Fig. 12. The original SAR image (2008-10-19, Changjiangkou precautionary, Envisat-1 ASAR HH)

Fig. 13. (left) The selected detecting zone (original image), (middle) The vessel detection results (the red cross), (right) Ship size identification and the heading direction estimation result

No.	Position	Type	Length(m)	Heading angle (degree)
1	123.5118E 38.4035N	M	99.3905	124.2916
2	123.8202E 36.0825N	M	80.3638	176.8479
3	124.2371E 31.8074N	M	98.8651	0.4757
4	124.2207E 38.8641N	M	92.0447	173.3593
5	124.441E 32.1691N	M	108.5735	89.9972
6	129.429E 35.3644N	M	95.7427	233.4018
7	129.5839E 33.1727N	L	140.0645	10.0805
8	129.8325E 36.7182N	L	116.6667	179.5634
9	130.0705E 35.3129N	XL	219.6904	0.0432
10	129.9275E 38.2278N	M	73.48	7.3131

Note: There are totally 44 vessels are detected, and only 10 are listed here.

Table 6. The vessel detection results

5.3.2 Performance analysis

- VTS vessel report: 51
- Detected vessel: 44
- Detecting rate: 86%
- Position error: 0.06 nmile

Among the detection, six small vessels and one middle sized vessel were missed. The performance is better in the detection of big and extra big vessels.

5.3.3 Sea state estimation

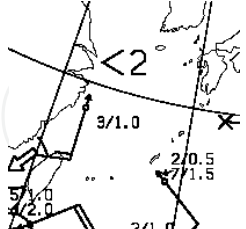The wave direction estimation result is shown in Table 7.

Acquisition Time (UTC)	Polarization Mode	Incident Angle	Estimated Direction	JMH Wave Analysis
20081019 13:56	HH/HV	44.0092	104.8161	

Table 7. The wave direction estimation result

5.3.4 Ship position prediction

- Ship number: 1 ♯
- Predicting time: 2 hours After
- Ship speed: 15 knot
- Flow speed: 3 knot
- MSR Searching region prediction:
  - Northwest: 123.1202E, 36.7825N;
  - Southeast: 124.5202E, 35.3825N.

5.4 The system performance

The complete maritime search and rescue system supplies the function of ship detection, identification and location algorithm. It can be also used to inquire the satellite transit time and its orbit data. The precision of ship size estimation reached over 80% and the position estimate the position detecting error is within 0.5 nautical miles.

6. Conclusion

In this chapter, a remote sensing monitoring system for maritime search and rescue (RS-MSR) is presented. Some related algorithms are introduced. The satellite remote sensing imageries of large scale water area are acquired to detect and locate distress ships for guiding the search operation. Some important data such as current and sea state are retrieved to assist decision-making of the operation. System experiment design and test are presented, and the performance shows that this system can effectively improve the searching speed and accuracy, and is of significance in promoting rescue success rate and efficiency.

7. Acknowledgment

8. References

Dare P., Dowman I. (2001). An Improved Model for Automatic Feature-based Registration of SAR and SPOT Images, *ISPRS Journal of Photogrammetry & Remote Sensing*, 2001, Vol.56, pp.13-28

Gerkacg J. (1999). Spatially Distributed Target Detection in Non-Gaussian Clutter. *IEEE Trans. on AES*, 1999, Vol.35, No.3, pp.926-934

Huang D.S & Han Y.Q. (1997). A Detection Method of High Resolution Radar Targets Based on Position Correction. *Journal of Electronics*, 1997, Vol.19, No.5, pp.584-590.

Kapoor R.; Banerjee A.; Tsihrintzis G.A. & et al. (1999). UWB Radar Detection of Target in Foliage using Alpha-stable Clutter Models. *IEEE Trans. on AES*, 1999, Vol.35, No.3, pp.819-833

Kuttikkad S. & Chllappa R. (1994). Non-Gaussian CFAR Techniques for Target Detection in High Resolution SAR Images. *IEEE, International Radar Conference 1994, pp.910-914*, Austin, TX, USA, 1994

Morrone, M.C. & Owens, R.A. (1987). Feature Detection from Local Energy, *Pattern Recognition Letters*, Vol. 6, pp. 303-313

Novak L.M. & Hesse S.R. (1993). Optimal Polarization for Radar Detection and Recognition of Targets in Clutter, *IEEE, National Radar Conference*, pp.79-83, Lynnfield, MA, USA, 1993

Steger, C. (1996). An Unbiased Detector of Curvilinear Structures, *Technical Report FGBV-96-03*, Forschungsgruppe Bildverstehen (FG BV), Informatik IX, Technische Universität München

Uratsuka S. & et al. (2002). High-resolution Dual-bands Interferometric and Polarimetric Airborne SAR (Pi-SAR) and Its Applications, *Proceedings of IGARSS'02*, Vol.3, pp.24-28

Remote Sensing - Applications

Edited by Dr. Boris Escalante

Nowadays it is hard to find areas of human activity and development that have not profited from or contributed to remote sensing. Natural, physical and social activities find in remote sensing a common ground for interaction and development. This book intends to show the reader how remote sensing impacts other areas of science, technology, and human activity, by displaying a selected number of high quality contributions dealing with different remote sensing applications.

How to reference

In order to correctly reference this scholarly work, feel free to copy and paste the following:

Jing Peng and Chaojian Shi (2012). Remote Sensing Application in the Maritime Search and Rescue, Remote Sensing - Applications, Dr. Boris Escalante (Ed.), ISBN: 978-953-51-0651-7, InTech, Available from: http://www.intechopen.com/books/remote-sensing-applications/remote-sensing-application-in-the-maritime-search-and-rescue

INTECH
open science | open minds